Atmos. Chem. Phys., 18, 8001–8016, 2018
https://doi.org/10.5194/acp-18-8001-2018

Atmospheric Chemistry and Physics
Open Access

Investigation of the oxidation of methyl vinyl ketone (MVK) by OH radicals in the atmospheric simulation chamber SAPHIR

Hendrik Fuchs[1], **Sascha Albrecht**[1], **Ismail–Hakki Acir**[1,a], **Birger Bohn**[1], **Martin Breitenlechner**[2], **Hans-Peter Dorn**[1], **Georgios I. Gkatzelis**[1], **Andreas Hofzumahaus**[1], **Frank Holland**[1], **Martin Kaminski**[1,b], **Frank N. Keutsch**[2], **Anna Novelli**[1], **David Reimer**[1], **Franz Rohrer**[1], **Ralf Tillmann**[1], **Luc Vereecken**[1], **Robert Wegener**[1], **Alexander Zaytsev**[2], **Astrid Kiendler-Scharr**[1], and **Andreas Wahner**[1]

[1]Institute of Energy and Climate Research, IEK-8: Troposphere, Forschungszentrum Jülich GmbH, Jülich, Germany
[2]School of Engineering and Applied Sciences and Department of Chemistry and Chemical Biology, Harvard University, Cambridge, MA, USA
[a]now at: Institute of Nutrition and Food Sciences, Food Chemistry, University of Bonn, Germany
[b]now at: Bundesamt für Verbraucherschutz, Abteilung 5 – Methodenstandardisierung, Berlin, Germany

Correspondence: Hendrik Fuchs (h.fuchs@fz-juelich.de)

Received: 12 March 2018 – Discussion started: 19 March 2018
Revised: 18 May 2018 – Accepted: 23 May 2018 – Published: 7 June 2018

Abstract. The photooxidation of methyl vinyl ketone (MVK) was investigated in the atmospheric simulation chamber SAPHIR for conditions at which organic peroxy radicals (RO_2) mainly reacted with NO ("high NO" case) and for conditions at which other reaction channels could compete ("low NO" case). Measurements of trace gas concentrations were compared to calculated concentration time series applying the Master Chemical Mechanism (MCM version 3.3.1). Product yields of methylglyoxal and glycolaldehyde were determined from measurements. For the high NO case, the methylglyoxal yield was (19 ± 3) % and the glycolaldehyde yield was (65 ± 14) %, consistent with recent literature studies. For the low NO case, the methylglyoxal yield reduced to (5 ± 2) % because other RO_2 reaction channels that do not form methylglyoxal became important. Consistent with literature data, the glycolaldehyde yield of (37 ± 9) % determined in the experiment was not reduced as much as implemented in the MCM, suggesting additional reaction channels producing glycolaldehyde. At the same time, direct quantification of OH radicals in the experiments shows the need for an enhanced OH radical production at low NO conditions similar to previous studies investigating the oxidation of the parent VOC isoprene and methacrolein, the second major oxidation product of isoprene. For MVK the model–measurement discrepancy was up to a factor of 2. Product yields and OH observations were consistent with assumptions of additional RO_2 plus HO_2 reaction channels as proposed in literature for the major RO_2 species formed from the reaction of MVK with OH. However, this study shows that also HO_2 radical concentrations are underestimated by the model, suggesting that additional OH is not directly produced from RO_2 radical reactions, but indirectly via increased HO_2. Quantum chemical calculations show that HO_2 could be produced from a fast 1,4-H shift of the second most important MVK derived RO_2 species (reaction rate constant $0.003\,s^{-1}$). However, additional HO_2 from this reaction was not sufficiently large to bring modelled HO_2 radical concentrations into agreement with measurements due to the small yield of this RO_2 species. An additional reaction channel of the major RO_2 species with a reaction rate constant of $(0.006 \pm 0.004)\,s^{-1}$ would be required that produces concurrently HO_2 radicals and glycolaldehyde to achieve model–measurement agreement. A unimolecular reaction similar to the 1,5-H shift reaction that was proposed in literature for RO_2 radicals from MVK would not explain product yields for conditions of experiments in this study. A set of H-migration reactions for the main RO_2 radicals were investigated by quantum chemical and theoretical kinetic methodologies, but did not reveal a contributing route to HO_2 radicals or glycolaldehyde.

Published by Copernicus Publications on behalf of the European Geosciences Union.

1 Introduction

Isoprene (C_5H_8) emitted by plants (Guenther et al., 2012) has the highest emission rate among non-methane organic compounds. Isoprene is mainly oxidised by the photochemically generated hydroxyl radical (OH) forming the first-generation organic compounds methacrolein (MACR), methyl vinyl ketone (MVK), formaldehyde (HCHO and isoprene hydroxyperoxides (ISOPOOH) (e.g. Karl et al., 2006). The latter ones are formed without the involvement of nitric oxide (NO) so that ISOPOOH becomes increasingly important with decreasing concentrations of nitrogen oxides (St. Clair et al., 2015) which are mainly released by anthropogenic activities. The formation of MVK and MACR is accompanied by the production of HO_2, which can further recycle OH, whereas ISOPOOH formation is a radical termination reaction. However, field studies have shown that also in environments where NO concentrations are less than a few 100 pptv a high OH regeneration rate can be maintained which is not explained by chemical models (Tan et al., 2001; Lelieveld et al., 2008; Hofzumahaus et al., 2009; Whalley et al., 2011). The gap between measured and modelled OH is correlated with the abundance of isoprene (Lu et al., 2012). Since then, it has been recognised that organic peroxy radical (RO_2) pathways which do not require NO as reaction partner can also significantly recycle OH (Wennberg et al., 2018). These reactions include

- hydrogen-shift reactions of RO_2 radicals forming OH or HO_2,
- reaction of peroxy radicals with HO_2.

These pathways have both been identified in the oxidation chain of isoprene (Peeters et al., 2009, 2014). A 1,6 H-shift of RO_2 formed in the reaction of isoprene with OH leads to the formation of hydroxyperoxy aldehydes (HPALD) and HO_2. The photolysis of HPALD gives even additional OH radicals. Its relevance for the atmosphere has been shown in laboratory experiments (Crounse et al., 2011; Wolfe et al., 2012) and chamber experiments (Fuchs et al., 2013). In the supplement of the first publication of the LIM (Peeters et al., 2009) the authors also suggested that a 1,5-H-shift reaction could be relevant for MVK and MACR. However, for MACR a 1,4 H-shift reaction for RO_2 was found, which efficiently recycles OH (Crounse et al., 2012). Its impact on the radical budget has been shown in chamber experiments (Fuchs et al., 2014). H-shift reactions have also been proposed to be important for RO_2 radicals which are formed in the oxidation chain of ISOPOOH (D'Ambro et al., 2017) also potentially enhancing the OH regeneration rate.

The reaction of peroxy radicals with HO_2 forms not only hydroxyperoxides, but also OH together with an alkoxy radical. This was shown for the acetylperoxy radical with an OH yield of 50 % (Dillon and Crowley, 2008; Winiberg et al., 2016). In a recent study by Praske et al. (2015), product yields from the reaction of MVK derived peroxy radicals with HO_2 were investigated. Similar to the acetylperoxy radical, product yields demonstrated that only one third of the reaction yields hydroxyperoxides and that two additional reaction channels exist, both of which could lead to the reformation of OH.

In this study, the oxidation of MVK by OH was investigated in the atmospheric simulation chamber SAPHIR (Simulation of Atmospheric Photochemistry In a Large Reaction Chamber) at Forschungszentrum Jülich. Experiments were performed under controlled conditions with atmospheric trace gas and radical concentrations. In these experiments, not only organic compounds like in previous studies were measured, but also radical species (OH, HO_2, and RO_2) allowing for an analysis of the OH budget. In the low NO case, NO mixing ratios were kept below 100 pptv so that different RO_2 radical reactions, i.e. reaction with HO_2 and unimolecular isomerisation reactions, can compete. Measured time series of radical concentrations are compared to model calculations applying the Master Chemical Mechanism version 3.1.1 (MCM, 2017) and modifications suggested in literature.

2 Methods

2.1 Simulation experiment in SAPHIR

Experiments were performed in the outdoor atmospheric simulation chamber SAPHIR. Details of the chamber can be found in previous publications (e.g. Rohrer et al., 2005). SAPHIR has a cylindrical shape (length 18 m, diameter 5 m, volume 270 m^3 and consists of a double-wall FEP (fluorethylene-propylene) film. A small overpressure (45 Pa) prevents ambient air entering the chamber. The replenishment flow that is required to maintain this pressure leads to a dilution of all trace gases by approximately 3 to 5 % per hour. A shutter system shades the chamber before the photooxidation experiment is started. Natural sunlight is used to irradiate the mixture. Small sources of nitrous acid (HONO) and formaldehyde (HCHO) are present in the sunlit chamber (100 to 200 pptv h^{-1}). The photolysis of HONO is typically the primary source for OH radicals and nitrogen oxides.

In total, four experiments were conducted in this study, two of them at low NO (23 June 2016: NO < 70 pptv and 23 May 2017: NO < 40 pptv) and two of them at high NO conditions (20 August 2014: 0.7 to 6 ppbv NO and 17 May 2017: approximately 0.1 to 0.4 ppbv NO). Results from experiments performed at similar conditions gave consistent results. The discussion of results focuses on the two experiments for which the number of trace gas measurements was highest and results for the other experiments are shown in the Supplement.

The experiments started with cleaning the chamber air by flushing out impurities from previous experiments until trace gas concentrations were below the detection limit of the instruments. The chamber air was first humidified by flushing water vapour from boiling water into the dark chamber (relative humidity approximately 70 %). In the low NO experiments, approximately 140 ppbv ozone produced from a silent discharge ozoniser (O3onia) was injected in the dark in order to suppress NO concentrations. In contrast, 6 to 10 ppbv of NO_2 or NO were injected from a gas mixture in case of the high NO experiments. In one of the two low NO experiments (23 May 2017), 20 ppbv MVK (Sigma-Aldrich, purity 99 %) in water was injected in the dark chamber from a Liquid Calibration Unit (LCU, Ionicon). MVK (1.5 ppbv) was reinjected after 3.5 h of photooxidation. In the other experiments, MVK was injected several times during the experiment after an initial phase of illumination of the chamber air without additional OH reactants by injecting liquid MVK into a heated inlet line that is flushed by synthetic air. This procedure was similar to that applied in previous studies (e.g. Fuchs et al., 2013, 2014; Kaminski et al., 2017). The photooxidation of MVK was then observed for several hours. No significant particle formation was observed in the experiments so that only gas-phase chemistry needs to be considered in the evaluation.

2.2 Instrumentation

Trace gas concentrations were measured with a comprehensive set of instruments. Nitric oxide (NO) was detected by chemiluminescence (Eco Physics) and nitrogen dioxide (NO_2) by the same instrument but with a blue-light converter in the inlet. In one of the experiments (17 May 2017), no NO_x measurements were available. A cavity ring-down instrument (Picarro) monitored water vapour and carbon monoxide and a UV photometer (Ansyco) detected ozone.

The total OH reactivity (inverse lifetime of OH) was measured by a pump-probe method (Lou et al., 2010; Fuchs et al., 2017), in which the decay of OH radicals produced by laser flash photolysis of ozone is observed by laser-induced fluorescence (LP-LIF). OH reactivity gives a measure of all OH reactant concentrations, so that potential gaps in the detection of e.g. organic compounds that are relevant for the radical chemistry can be identified (e.g. Nölscher et al., 2012). Unfortunately, the instrument failed in 2014, thus OH reactivity was only measured in one of the two high NO experiments.

Organic compounds were measured by a proton-transfer time-of-flight mass spectrometer (PTR-TOF-MS, Ionicon), which was calibrated to quantify MVK. Methylglyoxal ($CHOCOCH_3$, MGLYOX), and glycolaldehyde ($HOCH_2CHO$) were quantified in one low and one high NO experiment. In the other two experiments, performed in different years, the PTR-TOF-MS was calibrated for MVK, but not for methylglyoxal and glycolaldehyde for all experiments so that these species could not be quantified in all experiments. Acetic acid was detected on the same mass as glycolaldehyde in the PTR-TOF-MS instrument. However, model calculations suggest that the contribution of acetic acid was less than 10 % of the total signal. Therefore, measurements represent glycolaldehyde concentrations reasonably well.

A second PTR-TOF-MS instrument (PTR-3, Ionicon) quantified MVK concentrations in the experiment on 23 May 2017. Measurements of both instruments agreed within 20 %. In addition to direct measurements of MVK concentrations, measurements of the OH reactivity can be used to calculate the MVK concentration that was injected in the experiments because the increase in OH reactivity at that point in time can be attributed to the MVK concentration increase. The comparison with the increase in MVK measurements by the PTR-TOF-MS instrument shows good agreement.

In the experiments in 2017, formaldehyde was measured by the same differential optical absorption spectroscopy (DOAS) instrument that also detects OH radicals in the chamber (Dorn et al., 1995). In the other years, HCHO was measured by a Hantzsch monitor. The 1σ-precision of the formaldehyde measurement of 230 pptv is less than that of the Hantzsch monitor (20 pptv), but it is sufficiently high for the detection of HCHO in the experiments here.

OH was detected by DOAS (Dorn et al., 1995) in all experiments except for the high NO experiment in 2014. In addition, OH, HO_2 and RO_2 radicals were measured by laser-induced fluorescence (LIF). The instrument has been described in detail elsewhere (Fuchs et al., 2008, 2011, 2016). OH concentrations measured by LIF in the SAPHIR chamber have been shown to agree with measurements by DOAS in several comparison exercises (e.g. Schlosser et al., 2009; Fuchs et al., 2012). Good agreement was also observed in this work so that significant potential artefacts in the LIF detection scheme as reported for some instruments in the field (Mao et al., 2012; Novelli et al., 2014; Rickly and Stevens, 2018) can be excluded.

HO_2 and RO_2 are chemically converted to OH by the reaction with NO prior to OH detection by laser-induced fluorescence in the LIF instrument. The conversion of RO_2 requires at least two subsequent reactions with NO. First, RO_2 is converted through adding NO to HO_x in a flow reactor upstream of the fluorescence cell. Added CO in the reactor ensures that the HO_x consists predominantly of HO_2, which has a small wall loss compared to OH. The reactor is operated at higher pressure (25 hPa) compared to the low-pressure (4 hPa) LIF detection cell (Fuchs et al., 2009). The HO_x is sampled from the reactor into the LIF detection cell where HO_2 is converted by a large excess of added NO to OH. Operational parameters of the RO_2 system are optimized for the efficient detection of RO_2 radicals that have a similar reaction rate with NO as methylperoxy radicals. As a consequence, RO_2 radicals are not efficiently detected, if their reaction with NO does not directly and quantitatively result in the production of HO_2. This is for example the case for the peroxy radical $HMVKBO_2$ (as named in the MCM) that is formed from the reaction of MVK with OH (see below for details). This has

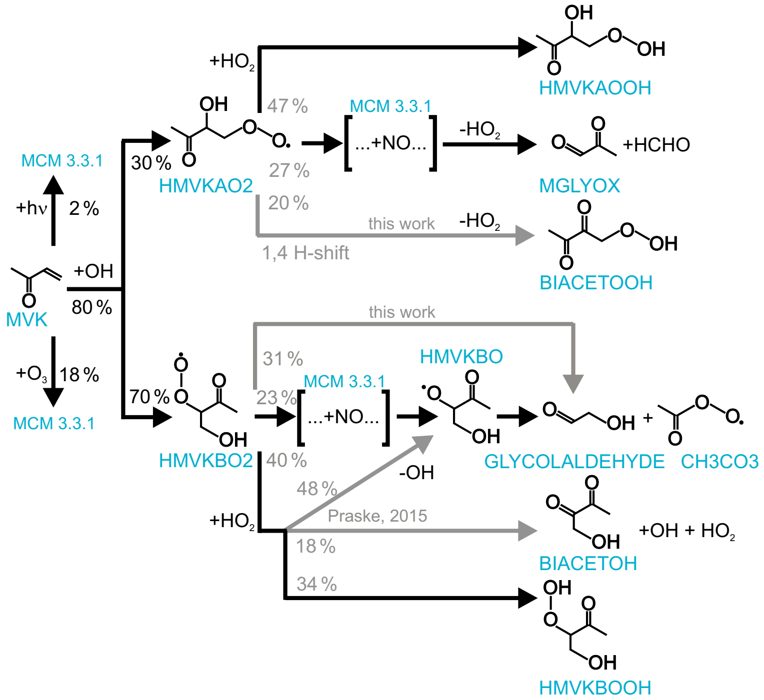

Figure 1. Simplified OH oxidation scheme for MVK. Names of compounds are assigned similar to MCM. Modifications to the MCM mechanism (M2) applied in model sensitivity runs M1 and M2 (Table 1) are shown as grey arrows. Reaction yields are calculated for conditions of the experiment with low NO (high ozone concentrations) on 23 May 2017. Grey numbers refer to model run M2.

to be taken into account, if measured RO_2 radicals are compared with model calculations.

The HO_2 detection cell consists of a fluorescence cell, in which HO_2 reacts with excess NO that is injected behind the inlet nozzle. As shown for several LIF instruments, the HO_2 signal can also contain contributions from RO_2 radicals that rapidly form HO_2 in the reaction with NO (Fuchs et al., 2011; Whalley et al., 2013; Lew et al., 2018). This applies for those RO_2 radicals which form an alkoxy radical (RO) in the reaction with NO that rapidly produces HO_2 and other products. The interferences from RO_2 can be minimised; however, if the instrument is operated with an NO concentration, for which the HO_2 to OH conversion efficiency is only approximately less than 10 %. In this case, the RO_2 to OH conversion efficiency becomes much smaller for all RO_2 species, because the two reactions with NO needed to produce OH limit the overall conversion efficiency. In this study, the HO_2 channel of the LIF instrument was operated such that RO_2 interferences can be assumed to be negligible.

In one of the experiments (23 May 2017), HO_2 was additionally detected by a newly developed chemical ionisation mass spectrometry (CIMS) instrument using Br^- as ionisation reagent. HO_2 is detected as cluster ion similar to the approaches reported by Veres et al. (2015); Sanchez et al. (2016) using an I^- and Br^- CIMS, respectively. Details of this new instrument will be presented in a separate publication. HO_2 measurements of the CIMS instrument agreed with $[HO_2]$ detected by the LIF instrument within 15 %.

Solar radiation was measured outside the chamber using a spectroradiometer. Photolysis frequencies are then calculated by applying a model to transfer outside conditions to conditions inside the chamber (Bohn et al., 2005; Bohn and Zilken, 2005). Latest recommendations for absorption spectra and photolysis yields are used.

2.3 Model calculations

Model calculations were performed using the Master Chemical Mechanism in its latest version 3.3.1 (MCM, 2017). A simplified reaction scheme is shown in Fig. 1. The MCM mechanism was modified (MCM*) to take results reported in literature into account and findings in this work. Details are listed in Table 1.

Chamber specific properties were added such as dilution of traces gases due to the replenishment flow. Sources for HONO and HCHO production from the chamber were parameterised as described in previous publications (e.g. Fuchs et al., 2014; Kaminski et al., 2017).

Model calculations were constrained to physical parameters (pressure, temperature, photolysis frequencies and dilution rate of trace gases). A small, constant background OH reactivity of unknown OH reactants that was measured by the OH reactivity instrument after humidification of the chamber

Table 1. Changes of reactions and additional reactions applied to the MCM.

	Reaction	Reaction rate constant	Reference
	MCM*:		
R1:	$OH + MVK \rightarrow HMVKAO_2$	$0.24 \times 2.6 \times 10^{-12} \exp(610\,K\,T^{-1})\ cm^3\,s^{-1}$	Praske et al. (2015)
R2:	$OH + MVK \rightarrow HMVKBO_2$	$0.76 \times 2.6 \times 10^{-12} \exp(610\,K\,T^{-1})\ cm^3\,s^{-1}$	Praske et al. (2015)
	$HOCH_2CHO + OH \rightarrow$ products	$8 \times 10^{-12}\ cm^3\,s^{-1}$	Karunanandan et al. (2007)
	$MVK + O_3 \rightarrow OH +$ products	$0.16 \times 8.5 \times 10^{-16} \exp(-1520\,K\,T^{-1})$	Aschmann et al. (1996), Paulson et al. (1998)
	M1 (includes MCM*):		
R3:	$HMVKBO_2 + HO_2 \rightarrow HMVKBOOH$	0.34×0.625 KRO2HO2[a]	Praske et al. (2015)
R4:	$HMVKBO_2 + HO_2 \rightarrow HMVKBO + OH$	0.48×0.625 KRO2HO2[a]	Praske et al. (2015)
R5:	$HMVKBO_2 + HO_2 \rightarrow BIACETOH + OH + HO_2$	0.18×0.625 KRO2HO2[a]	Praske et al. (2015)
	M2 (includes M1 and MCM*):		
R7:	$HMVKAO_2 \rightarrow HO_2 + BIACETOOH$	$0.003\ s^{-1}$[b]	This work
R8:	$HMVKBO_2\ (+X)$[c] $\rightarrow HO_2 + HOCH_2CHO + HCHO + CO$	$(0.006 \pm 0.004)\ s^{-1}$	This work
	$HOCH_2CO_3 + NO_2 \rightarrow PHAN$	0	This work

[a] value from MCM: $0.625\ KRO2HO2 = 2.91 \times 10^{-13} \exp(1300\,K\,T^{-1})\ cm^3\,s^{-1}$ (MCM, 2017) [b] from theoretical calculation (see Table 2). [c] A reaction partner could not be determined from these experiments.

air was modelled as an OH reactant that converts OH to HO_2. However, the magnitude of this background reactivity was small ($< 1\,s^{-1}$) compared to the OH reactivity from MVK during the experiment ($> 15\,s^{-1}$) so that it did not affect the chemistry.

Injections of trace gases were modelled as sources during the time of injection, but injected trace gases were not constrained to measured values at later times. [NO], [NO_2] and [O_3] were only constrained to measurements for the high NO_x experiment, because differences between modelled and measured values would have led to significant differences in other observables. No modelling could be performed for one of the high NO experiments (17 May 2017) due to the lack of NO_x measurements. No measurements for the reaction rate constants of RO_2 species from MVK exist. The sensitivity of model results to a change of the RO_2 reaction rate constants, however, is rather small so that their uncertainties could not explain observed model–measurements discrepancies.

2.4 Quantum-chemical calculations

A set of H-migration reactions for the main MVK-derived peroxy radicals was investigated by quantum chemical and theoretical kinetic methodologies. The reactions studied included migration of hydroxyl, $\alpha-$OH, and methyl H-atoms; direct HO_2 elimination forming an enol was also investigated (Table 2).

Several methodologies were applied, as detailed in the supporting information. From these data, the M06-2X/cc-pVTZ rovibrational data (Dunning, 1989; Zhao and Truhlar, 2008), with CCSD(T)/aug-schwartz4(DT) single point energy calculations extrapolated to the basis set limit (Purvis and Bartlett, 1982; Martin, 1996) were selected. All quantum chemical calculations were performed using the Gaussian-09 program suite (Frisch et al., 2010). The high-pressure rate coefficients for each of the elementary processes was then calculated using multi-conformer canonical transition state theory, MC-CTST (Vereecken and Peeters, 2003; Zheng and Truhlar, 2013) based on a rigid rotor harmonic oscillator paradigm, an exhaustive search of the reactants and TS conformers, and asymmetric Eckart tunnelling and WKB zero-curvature (ZCT) tunnelling. For the 1,4- and 1,6-H-shift in $HMVKAO_2$, a large difference between Eckart and ZCT tunnelling was found; the geometric average is reported here (see Supplement).

3 Results

3.1 Product yields

The reaction of OH with MVK leads to the addition of OH to either one of the double-bonded C-atoms so that two different RO_2 radical species can be formed (Fig. 1):

$$MVK + OH \rightarrow HMVKAO_2\ (\text{yield}: 0.3), \qquad (R1)$$

$$MVK + OH \rightarrow HMVKBO_2\ (\text{yield}: 0.7). \qquad (R2)$$

Yields are from current recommendations (Atkinson et al., 2006) that are also used in the MCM. The further reaction chain with NO gives glycolaldehyde and an acetylperoxy radical for $HMVKBO_2$ and methylglyoxal, formaldehyde and HO_2 for $HMVKAO_2$. In the low NO experiment

Table 2. H-migration and HO_2 elimination in hydroxy−MVK−peroxy radicals. Barrier height E_b, reaction energy E_{react} and the rate coefficient k at a temperature of 300 K are listed. Arrhenius expressions for a temperature range between 200 and 400 K are available in the Supplement.

Reactant	Reaction class	Product	E_b kcal mol^{-1}	E_{react} kcal mol^{-1}	k (300 K) s^{-1}
$HMVKAO_2$	−OH 1,5-H-shift	$CH_3-C(=O)-CH(O^\bullet)-CH_2OOH$	21.6	20.4	5.0×10^{-4}
	α−OH 1,4-H-shift	$CH_3-C(=O)-C^\bullet(OH)-CH_2OOH$	24.7	−6.2	3.3×10^{-3}
	$-CH_3$ 1,6-H-shift	$C^\bullet H_2-C(=O)-CH(OH)-CH_2OOH$	23.1	10.2	5.9×10^{-4}
$HMVKBO_2$	−OH 1,5-H-shift	$CH_3-C(=O)-CH(OOH)-CH_2O^\bullet$	22.5	20.6	8.8×10^{-5} [a]
	α−OH 1,4-H-shift	$CH_3-C(=O)-CH(OOH)-C^\bullet HOH$	25.1	6.5	3.2×10^{-5}
	$-CH_3$ 1,6-H-shift	$C^\bullet H_2-C(=O)-CH(OOH)-CH_2OH$	27.4	10.0	3.8×10^{-5}
	HO_2 elimination	$CH_3-C(=O)-CH=CHOH + HO_2$	30.0	−1.5	6.1×10^{-10}

[a] estimated at 0.01 s^{-1} by Peeters et al. (2009).

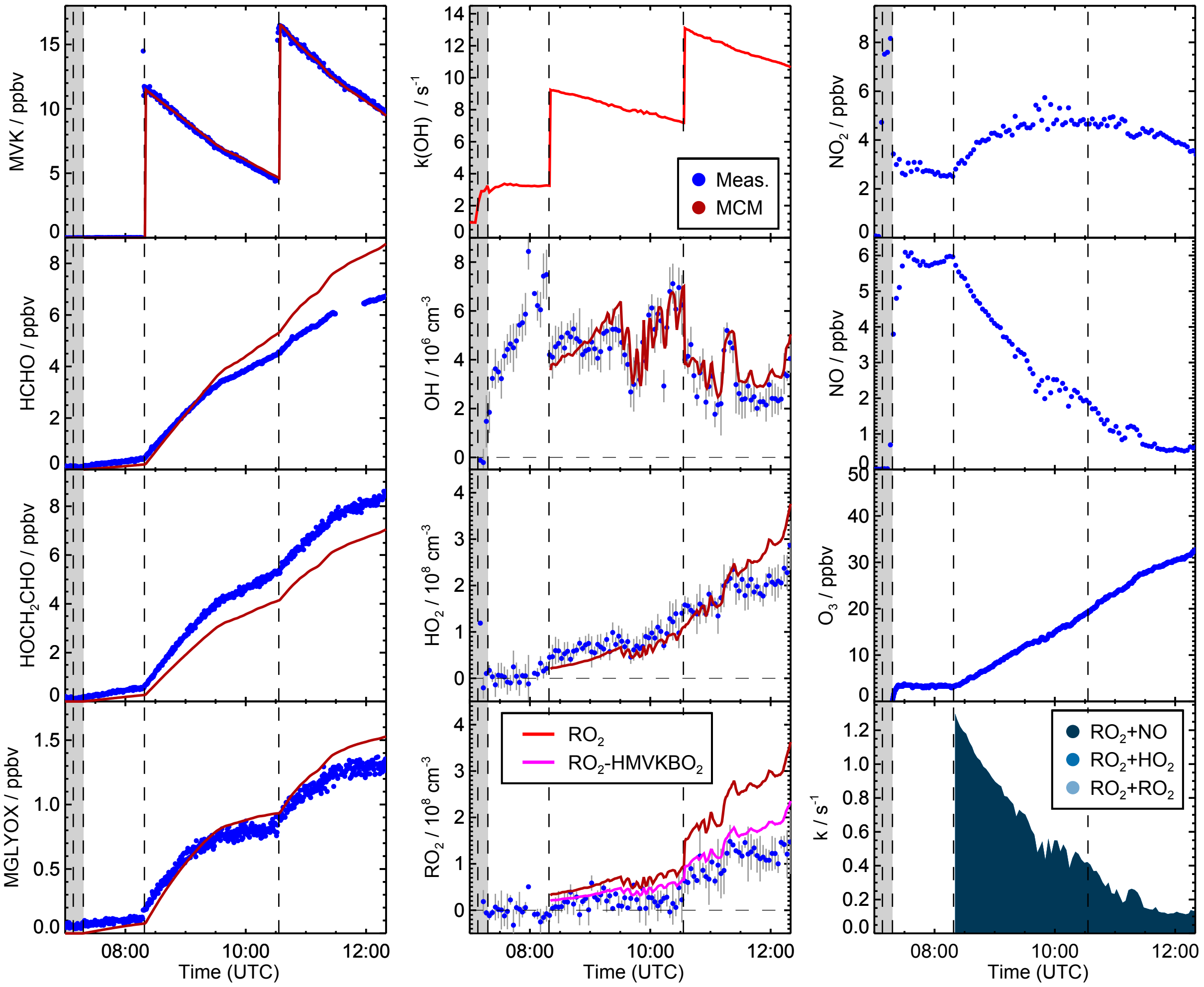

Figure 2. Time series of radicals, inorganic and organic species during the MVK photooxidation for the high NO experiment (20 August 2014) together with results from model calculations applying MCM. Dark shaded areas indicate the time before opening the chamber roof and vertical dashed line times when trace gases were injected into the chamber. OH reactivity was not measured during this experiment. NO, NO_2 and O_3 are constrained to measurements in the model. RO_2 loss rates (most lowest right panel) are calculated from modelled HO_2, RO_2 and NO concentrations. However, contributions from the reactions with RO_2 and HO_2 or RO_2 are too small to be visible. Modelled acetic acid concentrations are small compared to modelled glycolaldehyde concentrations (measured together in the PTR-TOF-MS).

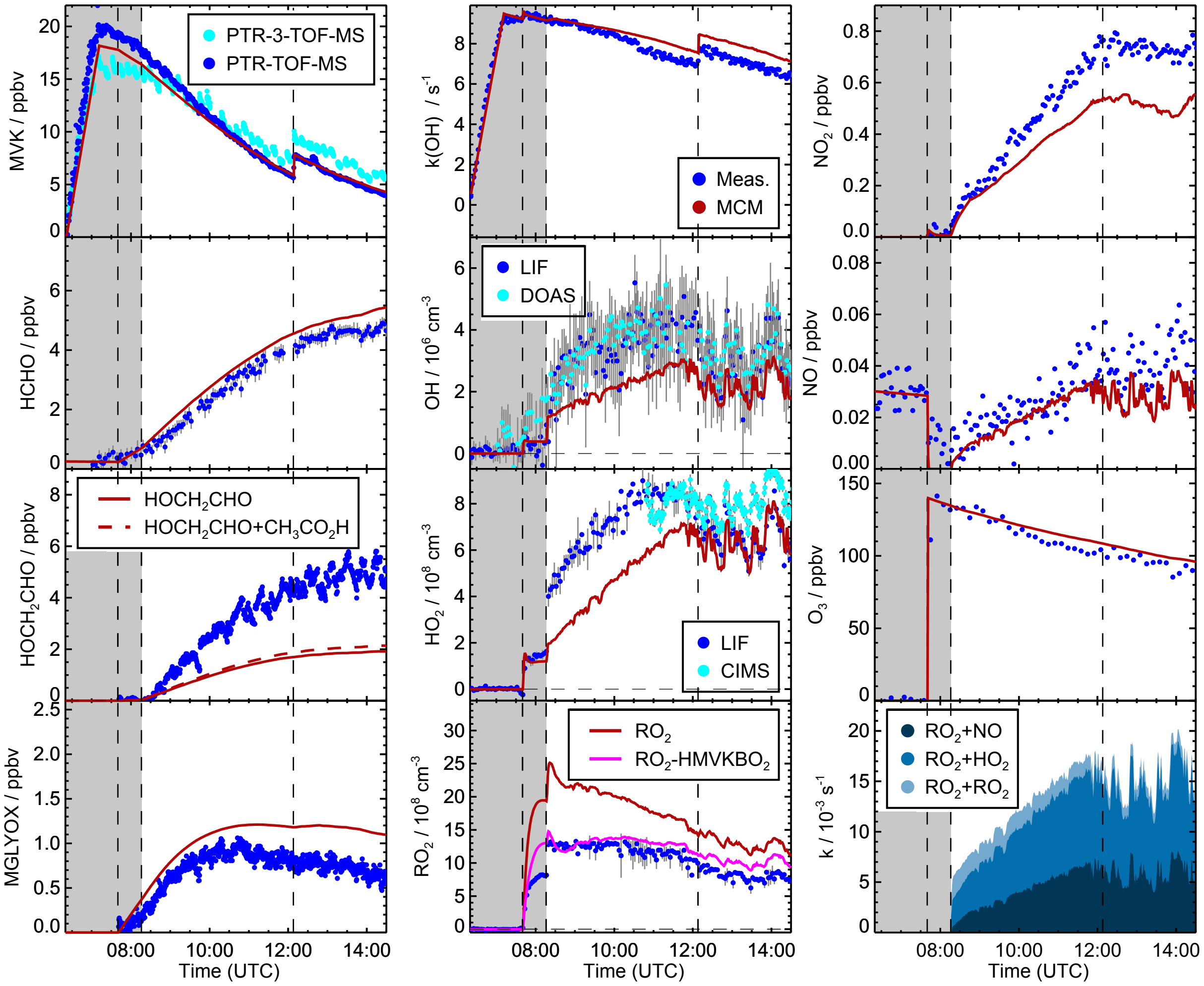

Figure 3. Time series of radicals, inorganic and organic species during the MVK photooxidation at low NO (23 May 2017) together with results from model calculations applying MCM. Dark shaded areas indicate the time before opening the chamber roof and vertical dashed line times when trace gases were injected into the chamber. RO_2 loss rates (most lowest right panel) are calculated from modelled HO_2, RO_2 and NO concentrations.

(23 May 2017), approximately 30 % of the RO_2 reacted with NO assuming that the reaction with HO_2 was the only competing reaction. In contrast, more than 90 % of RO_2 reacted with NO in the high NO experiment. Mixing ratios of the major products formaldehyde, glycolaldeyde and methylglyoxal increased to 6, 8, and 1.3 ppbv, respectively, in the high NO experiment when 13 ppbv MVK was oxidised (Fig. 2). Less of these products was observed in the low NO experiment with 4.5 ppbv formaldehyde, 5 ppbv glycolaldehyde and 1 ppbv methylglyoxal (Fig. 3) when 17 ppbv MVK is oxidised. The smaller concentrations of these products in the low NO case might be expected, because other products can be formed in the competing RO_2 reaction channels (Fig. 1).

Because part of the products are oxidised during the experiment, a correction procedure described in detail by Galloway et al. (2011) and Kaminski et al. (2017) is applied, in order to calculate products yields originating from the oxidation of MVK. This correction takes loss of products due to the reaction with OH and photolysis into account and also small production from chamber sources. The relationship between consumed MVK and corrected product concentrations gives the yield of the product species (Table 3, Fig. S3).

For the high NO experiment, when RO_2 nearly exclusively reacted with NO, the ratio of product yields for glycolaldehyde (0.65 ± 0.14) and methylglyoxal (0.19 ± 0.03) can be related to the branching ratio of the MVK reaction with OH (Reactions R1 and R2), because these products are formed in either one of the two reaction channels. The values derived from this experiment agree within their uncertainties with studies by Galloway et al. (2011), Tuazon and Atkinson (1989), and Praske et al. (2015) all reporting lower methylglyoxal yields than suggested by current recommendations (Atkinson et al., 2006). This indicates that the branching ratio assumed in the MCM of 0.7 : 0.3 needs to be shifted to-

Table 3. Yields of organic products from photooxidation of MVK by OH from this work and from the literature. Errors of values from this work take into account the accuracy of measurements and precision of the calculation. HCHO is not only produced in the first oxidation step of MVK but also produced in the subsequent oxidation of glycolaldehyde and methylglyoxal. Therefore, the yield can increase over the course of the experiment.

Species	Yield	$\frac{\text{loss}(RO_2+HO_2)}{\text{loss}(RO_2+NO)}$	Reference
HCHO	0.24 ± 0.08[a]	2 : 1[c]	This work
	0.46 ± 0.04[b]	2 : 1[c]	This work
	0.73 ± 0.15	1 : 9	This work
	0.54 ± 0.04	0:1	Tuazon and Atkinson (1989)
	0.28	0 : 1	Grosjean et al. (1993)
MGLYOX	0.05 ± 0.02	2 : 1[c]	This work
	0.04 ± 0.01	1 : 0	Praske et al. (2015)
	0.19 ± 0.03	1 : 9	This work
	0.24 ± 0.001	0 : 1	Galloway et al. (2011)
	0.25 ± 0.08	0 : 1	Tuazon and Atkinson (1989)
	0.32	0 : 1	Grosjean et al. (1993)
$HOCH_2CHO$	0.37 ± 0.09	2 : 1[c]	This work
	0.38 ± 0.05	1 : 0	Praske et al. (2015)
	0.65 ± 0.14	1 : 9	this work
	0.74 ± 0.06	0 : 1	Praske et al. (2015)
	0.67 ± 0.04	0 : 1	Galloway et al. (2011)
	0.64 ± 0.16	0 : 1	Tuazon and Atkinson (1989)
	0.60	0 : 1	Grosjean et al. (1993)

[a] approximately after 1 h of oxidation. [b] after 3 h of oxidation. [c] $RO_2 + RO_2$ contribution to the total RO_2 loss: <20 %.

wards $HMVKBO_2$. Praske et al. (2015) suggests a branching ratio of 0.76 : 0.24. The formaldehyde yield of 0.73 ± 0.15 is higher than the methylglyoxal yield, because formaldehyde is not only a co-product of methylglyoxal in the reaction chain of $HMVKAO_2$ (Fig. 1), but can also be formed from secondary products in the oxidation scheme of MVK. This might also explain why the HCHO yield in this chamber experiment is higher than that in the study by Tuazon and Atkinson (1989). Product yields reported by Grosjean et al. (1993) differ for all three species (largest difference for formaldehyde) from the other studies for unclear reasons.

In the low NO case, other RO_2 reaction channels than reaction with NO gain in importance. Lower yields of methylglyoxal (0.05 ± 0.002) and glycolaldehyde (0.37 ± 0.09) compared to the high NO experiment are therefore found in this case. However, the relative decrease of glycolaldehyde is much smaller than that of methylglyoxal. This indicates that glycolaldehyde is also formed from other reaction channels than the reaction of $HMVKBO_2$ with NO. This agrees with results reported by Praske et al. (2015). In that study, a glycolaldehyde yield of 0.38 ± 0.05 was determined in experiments, in which RO_2 exclusively reacted with HO_2.

3.2 Modelled and measured time series of radical concentrations

Time series of trace gas and radical concentrations are shown together with model calculations using the MCM without modifications for one of the high NO experiments (Fig. 2, 20 August 2014) and for one of the low NO experiments (Fig. 3, 23 May 2017). Although the instrumentation that performed measurements in the experiments were partly different specifically for experiments done in different years, consistent results are obtained. In addition, parameters that are measured by two instruments agree within their combined uncertainties.

MVK (12 ppbv) was injected twice into the sunlit chamber in the high NO experiment (Fig. 2). Approximately half of the MVK reacted away before the second MVK addition was done. The NO mixing ratio decreased over the course of the experiment from nearly 6 to 0.5 ppbv, but was sufficiently high that 90 % of HO_2 reacted with NO for most of the time. OH concentrations ranged from $(2–4) \times 10^6\,\text{cm}^{-3}$ modulated by changes of the OH reactivity and radiation. Model calculations of [OH] agree with measurements within 20 % at all times during the oxidation of MVK. This corresponds to a good description of the measured MVK concentration by the model (deviations less than 5 %) demonstrating that the OH concentration fits the observed oxidation rate of MVK.

HO_2 and RO_2 radical concentrations were rather small ($< 2 \times 10^8\,cm^{-3}$) due to their fast loss in the presence of high NO. Measured and modelled HO_2 concentrations show good agreement until the NO mixing ratio decreased below 0.5 ppbv (at 11:00, Fig 2). In the case of RO_2, the model yields significantly larger concentrations than measurements. This discrepancy is plausible due to the incomplete conversion of the peroxy radical $HMVKBO_2$ in the pre-reactor. The transformation to HO_2 requires more than one NO reaction step and therefore remains incomplete during the transit through the reactor. If the modelled concentration of $[HMVKBO_2]$ is subtracted from the total modelled $[RO_2]$, good model–measurement agreement is obtained.

Overall, the good agreement between modelled and measured radical concentrations demonstrates that radical chemistry during the oxidation of MVK is well described by state-of-the-art chemical models, if RO_2 radicals are mainly lost in the reaction with NO.

In the low NO experiment (Fig. 3), approximately 20 ppbv of MVK was injected, before photooxidation started. As a consequence of the low NO (< 40 pptv), RO_2 radicals formed in the reaction of MVK with OH not only reacted with NO, but reaction with HO_2 and RO_2 were competitive. Model calculations using the MCM (Fig. 3) suggest that at least half of the RO_2 reacted with HO_2 and a smaller fraction (10 to 20 %) with other RO_2 radicals.

After nearly 6 h of oxidation, only 4 ppbv MVK was left in the presence of $(2–4)\times 10^6\,cm^{-3}$ OH. The amount of MVK that is injected in the model is adjusted to the increase in OH reactivity during the time of injection. The 10 % discrepancy to measured MVK mixing ratios is within the uncertainty of the PTR-TOF-MS calibration. However, the decay of the measured [MVK] is slightly faster than the decay in the model specifically during the first 2 h of oxidation. This corresponds to modelled OH concentrations, which are up to a factor of 2 smaller than measured OH concentrations during this time. At later times of the experiment, measured and modelled [OH] as well as the relative change in [MVK] are matched. Differences between measured and modelled OH concentrations in the first phase of the experiment are accompanied by HO_2 concentrations, which are approximately $2 \times 10^8\,cm^{-3}$ lower in the model compared to measured values. Measured $[HO_2]$ increased from $(4–8)\times 10^8\,cm^{-3}$ during the first 2 h. Modelled values match measurements at later times of the experiment like observed for [OH]. The concurrent underestimation of [OH] and $[HO_2]$ suggests that a radical source is missing in the model.

In a sensitivity run (MCM*), modifications of reactions that are reported in literature, but do not directly affect the fate of RO_2 are implemented:

- The reaction rate constant of glycolaldehyde with OH is lowered by 20 % following measurements by Karunanandan et al. (2007).
- Following the results of the product analysis (see above), the branching ratio of Reaction (R1) and R2 is changed from 0.3 : 0.7 to 0.24 : 0.76 as suggested by Praske et al. (2015).
- OH yield from ozonolysis of MVK is lowered to 16 % as determined by Aschmann et al. (1996) and Paulson et al. (1998) compared to 36 % assumed in the MCM.

Details are listed in Table 1. Differences with results with the current version of the MCM are rather small (not shown here) so that these modifications do not significantly affect the model–measurement agreement. They are included in the sensitivities model runs shown below.

4 Discussion

4.1 Additional $RO_2 + HO_2$ reactions

Product yields indicate that an additional source for glycolaldehyde that is not included in the MCM is required to explain observations in the low NO experiment. This is consistent with chamber experiments by Praske et al. (2015), which were performed under conditions that RO_2 exclusively reacted with HO_2. In this case, the glycolaldehyde yield is expected to be small, because glycolaldehyde is mainly formed in the subsequent reaction of RO_2 with NO (Fig. 1). In that study, also a $C_4\alpha-$diketone ($CH_3COCOCH_2OH$, MCM name: BIACETOH) was measured with a yield of 0.14. From these product yields, the authors suggest that there are reaction channels of the $HMVKBO_2$ plus HO_2 reaction in addition to the formation of hydroxyperoxides (Praske et al., 2015):

$$HMVKBO_2 + HO_2 \rightarrow HMVKBOOH \quad (\text{yield}: 0.34), \tag{R3}$$

$$HMVKBO_2 + HO_2 \rightarrow HMVKBO + OH \quad (\text{yield}: 0.48), \tag{R4}$$

$$HMVKBO_2 + HO_2 \rightarrow BIACETOH + OH + HO_2 \quad (\text{yield}: 0.18), \tag{R5}$$

Including Reactions (R3)–(R5) in the MCM* mechanism (M1 Table 1) results in an improved description of observations for the low NO experiment (Fig. 4). Modelled [OH] agrees with measurements within 20 %. The largest increase of modelled [OH] is obtained 1 to 2 h after starting the oxidation due to the additional radical regeneration from Reactions (R4) and (R5). The model–measurement agreement is worsened for $[RO_2]$ compared to the MCM model run, but still within the uncertainty of the measurement. The additional production of glycolaldehyde from the subsequent chemistry of Reaction (R4) brings modelled organic product species into agreement with measurements within 20 % so that all observations except for $[HO_2]$ can be explained by the new reactions of $HMVKBO_2$ with HO_2. HO_2 concentrations,

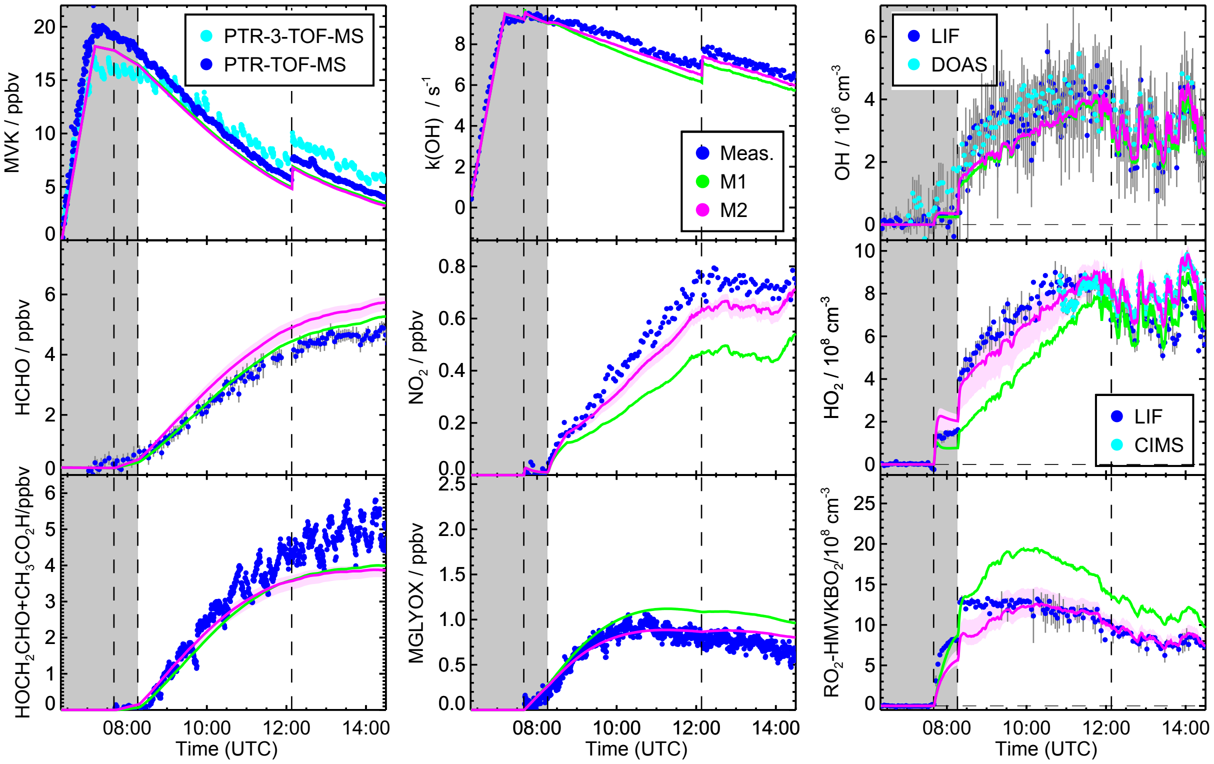

Figure 4. Time series of radicals, inorganic and organic species during the MVK photooxidation at low NO (experiment on 23 May 2017). Dark shaded areas indicate the time before opening the chamber roof and vertical dashed line times when trace gases were injected into the chamber. Model sensitivity runs M1 and M2 include modifications listed in Table 1.

however, are still significantly lower in the model compared to measurements. Results are consistent with experiments by Praske et al. (2015), but a potential underestimation of [HO_2] could not be recognised, because HO_2 radicals were not measured in their experiments.

4.2 RO_2 isomerisation reactions

RO_2 isomerisation reactions have been shown to be of importance for the atmospheric fate of RO_2 from isoprene (Peeters et al., 2014). Peeters et al. (2009) also suggested from quantum-chemical calculations that $HMVKBO_2$ undergoes a fast 1,5-H shift with subsequent decomposition (Fig. 1 and Table 1):

$$HMVKBO_2 \rightarrow MGLYOX + HCHO + OH. \qquad (R6)$$

Here, the possibility of RO_2 isomerisation reactions for both major RO_2 species formed from the reaction of MVK with OH were investigated in detail by means of quantum-chemical calculations.

Table 2 shows the reaction pathways that were examined for the $HMVKAO_2$ and $HMVKBO_2$ peroxy radicals. More information can be found in the Supplement. For both radicals, 1,5-H-migration of the hydroxyl H-atom is energetically most favourable with a barrier of 22 $kcal\,mol^{-1}$. The predicted reaction rate constant remains below $5 \times 10^{-4}\,s^{-1}$, mostly due to limited tunnelling owing to the large reaction endothermicity, and the broad energy barrier protruding less than 2 $kcal\,mol^{-1}$ above the reaction products. The concomitant low energy barrier for the reverse H-migration in the product implies that the reaction might be competitive against the alkoxy product decomposition with estimated barriers 4 $kcal\,mol^{-1}$ (Vereecken and Peeters, 2009). Most of the other reactions considered are several orders of magnitude slower and can be neglected. The predicted rates for all processes considered remain over an order of magnitude below that required to fit the measured OH, HO_2 and glycolaldehyde concentrations so that these H-migration reactions do not have a discernible impact on the MVK oxidation chemistry radical budget or product yields at room temperature. As such, the subsequent chemistry after these reactions was not investigated.

The isomerisation rate constant estimated by Peeters et al. (2009) for Reaction (R6) of 0.01 s^{-1} is about two orders of magnitude faster than calculated here. This is mainly related to the higher energy barriers found at the levels of theory applied in this work. The small reaction rate constant for this reaction is consistent with the small product yield for methylglyoxal found in the low NO experiment, which would need to be significantly higher than calculated, if Reaction (R6) was competitive with the other RO_2 reaction channels. A similar conclusion was drawn from product yields obtained in the study by Praske et al. (2015).

The fastest reaction rate coefficient of RO_2 isomerisation reactions calculated here is found to be the $HMVKAO_2$ 1,4-H-migration of the hydrogen atoms adjacent to the $-OH$ group, followed by H abstraction at the $-OH$ site by O_2 forming HO_2 together with a bi-ketone (named BIACETOOH in the MCM):

$$HMVKAO_2 + (O_2) \rightarrow HO_2 + BIACETOOH. \quad (R7)$$

A reaction rate constant of $0.003\,s^{-1}$ is calculated making this reaction competitive with the reaction of $HMVKAO_2$ with HO_2 and NO in the low NO experiments. Approximately 20 to 30 % of the $HVMKAO_2$ undergoes the 1,4-H shift reaction in this experiment. However, the resulting increase of the HO_2 concentration is rather small ($< 0.5 \times 10^8\,cm^{-3}$) because of the small $HMVKAO_2$ yield in the reaction of MVK with OH. This reaction is included in the model sensitivity runs M2.

4.3 Potential additional RO_2 reaction channel

A fast conversion of $HMVKBO_2$ to HO_2 would be required to fit HO_2 measurements. Glycolaldehyde would need to be a co-product to match measured values:

$$HMVKBO_2 + (X) \rightarrow HO_2 + \text{products} \quad (R8)$$

X represents an unknown reaction partner not needed in case of a unimolecular reaction. M2 in Fig. 4 gives the model result, if Reaction (R8) is included in the MCM* in addition to the 1,4-H shift of $HMVKAO_2$ (Reaction R7) and the additional channels of the reaction of $HMVKBO_2$ with HO_2 (Reactions R3–R5).

In order to fit HO_2 and glycolaldehyde concentration measurements, a reaction rate constant of $0.006 \pm 0.004\,s^{-1}$ is required. This reaction rate makes the Reaction (R8) competitive with the reaction of RO_2 with NO (reaction rate approximately $0.004\,s^{-1}$) and HO_2 (reaction rate approximately $0.008\,s^{-1}$). In M2, 40 % of $HMVKBO_2$ reacts with HO_2 and 30 % of $HMVKBO_2$ forms directly HO_2 and glycolaldehyde in Reaction (R8) for conditions of this experiment. In comparison, 60 % of $HMVKBO_2$ reacts with HO_2 in the model run M1. However, the overall effect on the [OH] is similar in both model runs so that modelled [OH] becomes consistent with measurements. This is due to the conversion of HO_2 produced in Reaction (R8) to OH. Overall, however, the major difference in the results of M1 and M2 is in the improved model–measurement agreement of $[HO_2]$.

Unfortunately, experiments here do not give hints about the exact nature of Reaction (R8). Quantum-chemical calculations (see above) shows that Reaction (R8) cannot be a unimolecular reaction such as H-atom migration, because they are not fast enough to compete with other RO_2 reaction channels. Photolysis of RO_2 that could results in OH/HO_2 have been observed for acetylperoxy radicals (Cox et al., 1990) and isoprene derived RO_2 (Hansen et al., 2017). However, the reaction rate constant of $0.006 \pm 0.004\,s^{-1}$ needed here to explain observations would require an unrealistically high absorption cross section. A reaction partner in Reaction (R8) could also be a RO_2 radical. However, in this case products of the $HMVKBO_2$ plus RO_2 reaction that are assumed in the MCM would need to be changed according to Reaction (R8) and the reaction rate constant would need to be increased by a large factor of 20 to 50 compared to recommendations for RO_2 self-reaction rate constants in order to make this reaction competitive with the other RO_2 reaction channels.

4.4 Model–measurement agreement of nitrogen oxide species

So far, only radicals and organic products have been discussed. However, there is also disagreement between measured and modelled NO_2 mixing ratios. The NO_2 concentration produced by the model is 30 % smaller in the low NO experiment (23 May 2017)) compared to measured values. This discrepancy increases to 40 %, if the OH concentration and therefore the MVK oxidation rate is increased. This is due to the increased production of peroxy radicals, which form peroxy acyl nitrate (PAN) or PAN like species, which act as nitrogen oxide reservoirs. Acetylperoxy radicals forming PAN are mainly produced from $HVMKBO_2$ as a co-product of glycolaldehyde, but another PAN-like species (MCM name PHAN) is additionally produced by the oxidation of glycolaldehyde. If no production of PHAN is assumed, measured and modelled NO_2 mixing ratios agree within 100 pptv (M2 in Fig. 4), less than the accuracy of the NO_x formation in the chamber. However, also reduction of the production of acetylperoxy radicals could improve the model–measurement agreement. The change in NO and peroxy radical concentrations is rather small, because of the suppression of NO by O_3 and the overall small turnover rate of HO_2 and NO. More specific experiments concerning the NO_x budget would be required to decide, which NO_x reservoir species is overestimated by the model.

4.5 OH budget analysis

OH is in steady state because of its short lifetime, so that its rates of production and destruction are equal. Therefore, OH reactivity together with OH concentration measurements allows determination of the total OH production rate from only two measured quantities. Under conditions with high NO concentrations, only few chemical reactions are typically controlling the OH production. The dominating process is usually the recycling of HO_2 by its reaction with NO. In addition, photolysis of ozone and HONO make significant contributions. For low NO conditions and in the presence of high VOC concentrations, field and chamber experiments often show larger total OH productions rates (derived from mea-

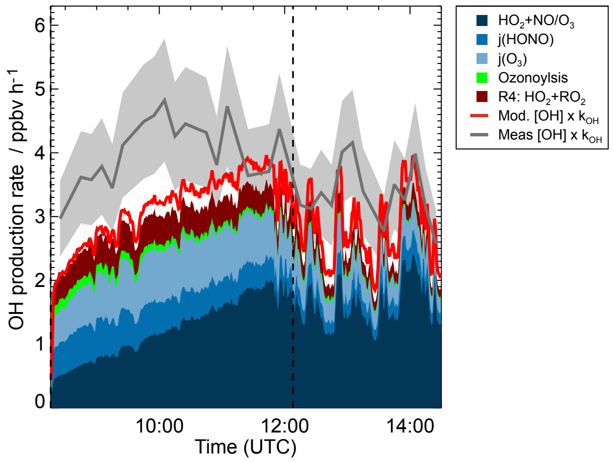

Figure 5. OH budget during the experiment at low NO concentration (23 May 2017) for the period, when MVK photooxidation took place. The vertical dashed line indicates when MVK was reinjected into the chamber. Red and blue coloured areas add contributions to the OH production calculated from the model results (M2 sensitivity run in Fig. 4). The contribution $RO_2 + HO_2$ refers to the OH production from Reaction (R4). In addition to modelled OH production contributions, total OH production calculated from the product of OH concentration and OH reactivity (k_{OH}) is shown. These quantities are either taken from the model results (M2) or from measurements. The coloured grey area gives the uncertainty of the total OH production calculation, if measured OH concentrations and measured OH reactivity are used.

sured OH and OH reactivity) than can be explained by the above processes. Under these conditions, other OH sources linked to the degradation of VOCs become relevant.

Figure 5 shows the OH budget for the low NO experiment (23 May 2017) using model results (M2, Table 1) to calculate contributions to the OH production. In addition, total OH production is calculated from measured and modelled OH concentrations and OH reactivity. Results from calculations using either modelled or measured values give similar numbers that agree within the uncertainty of the calculation of 20 %.

The OH production rate is dominated by HO_2 recycling reactions and primary OH production (HONO and O_3 photolysis). These contributions explain 70 to 80 % of the total OH production during the MVK oxidation. The model would give lower OH production compared to calculations using measurements if Reaction (R8) was not included because HO_2 concentrations and therefore OH recycling by HO_2 would be underpredicted in this case. This reaction is responsible for approximately half of the HO_2 concentration during the first 2 h of MVK oxidation. This demonstrates the importance of including all HO_2 sources in models.

Another 10 to 15 % of the total OH production rate is due to the OH formation from the additional HO_2 plus RO_2 reaction channel suggested by Praske et al. (2015) (Reaction R4). A large number of other OH forming reactions included in the model such as photolysis of hydroxyperoxides fills the remaining gap between these major contributions and the total calculated OH production.

5 Summary and conclusions

The photooxidation of MVK, one of the major oxidation products of isoprene, was investigated at atmospheric conditions in the simulation chamber SAPHIR. NO was varied from high to low concentrations. For high NO, RO_2 is mainly lost in the reaction with NO and current chemical models can describe radical concentrations within 20 %. Product yields of the major oxidation products glycolaldehyde (0.65 ± 0.14) and methylglyoxal (0.19 ± 0.03) are consistent with previous measurements (Tuazon and Atkinson, 1989; Galloway et al., 2011; Praske et al., 2015).

OH radical concentrations are underestimated (maximum factor 2) by the MCM at low NO concentrations (< 100 pptv), when other RO_2 reaction channels can compete with the reaction of RO_2 with NO. At the same time, also HO_2 and glycolaldehyde concentrations are smaller in the model compared to measurements. Only part of the model–measurements discrepancies can be explained by findings in recent studies investigating the MVK photooxidation. The higher glycolaldehyde yield is consistent with a study by Praske et al. (2015). The additional channels for the RO_2 plus HO_2 reaction suggested by these authors can reproduce glycolaldehyde and OH concentrations, but do not explain the model–measurement discrepancy for [HO_2].

The possibility of RO_2 isomerisation reactions for both major RO_2 species formed from the reaction of MVK with OH were investigated in detail by means of quantum-chemical calculations. Additional HO_2 can be produced from the 1,4-H shift reaction of $HVMKAO_2$. The reaction rate constant of 0.003 s^{-1} is competitive with other RO_2 reaction channels at low NO conditions. The overall impact, however, is small due to the small $HMVKAO_2$ yield. Other reactions considered here can be neglected for atmospheric conditions. This also includes the isomerisation reaction suggested by Peeters et al. (2009) (Reaction R6). The rate constant for this reaction is about two orders of magnitude smaller than calculated by Peeters et al. (2009) due to the higher energy barriers found at the higher levels of theory applied in this work.

Because HO_2 and glycolaldehyde concentrations are underestimated at the same time, a reaction that converts RO_2 to HO_2 and glycolaldehyde (Reaction R8) would explain observations in these experiments. A reaction rate constant of $0.006 \pm 0.004\ s^{-1}$ is required to bring measured and modelled values into agreement. Unimolecular H-shift reactions are found to be too slow. Alternatively, reaction of $HMVKBO_2$ with RO_2 that would produce directly HO_2 and glycolaldehyde would explain [HO_2] observations and would give similar OH and glycolaldehyde concentrations as the mechanism by Praske et al. (2015). However, more than the product species would need to be different from what is described in the MCM, but also the reaction rate constants would need to be increased by a large factor of 20 to 50 for the $HMVKBO_2$ plus RO_2 reaction. More studies will be needed to explore the exact role of HO_2 in the MVK oxidation scheme. In addition, open questions remain concerning the fate of nitrogen oxides in the MVK oxidation scheme. The MCM suggests the built-up of nitrogen oxide reservoirs by the formation of PAN and PAN-like species. Experiments here indicate that these reservoirs are less important.

The need for an additional HO_2 source was also found in the oxidation of monoterpenes. Field studies, in which OH reactivity was dominated by monoterpenes, showed that models underestimate HO_2 and OH concentrations (Kim et al., 2013; Hens et al., 2014). A chamber study investigating the photochemistry of $\beta-$pinene found that an additional HO_2 source is required to explain observed HO_2 and OH and suggested a rearrangement of radical intermediates as explanation (Kaminski et al., 2017).

The impact on the OH recycling efficiency and observed organic products in the MVK oxidation are the same regardless whether OH is directly produced from HO_2 plus RO_2 like in the Praske et al. (2015) mechanism or if OH is produced from enhanced HO_2 as suggested by experiments here. The enhanced OH recycling is demonstrated in this study by the direct quantification of the OH radical concentration during the photochemical oxidation of MVK. Similar as for isoprene (Peeters et al., 2014; Fuchs et al., 2013) and the second major organic product from isoprene oxidation, methacrolein, (Crounse et al., 2011; Fuchs et al., 2014), HO_x radicals are faster recycled in the MVK oxidation scheme than previously assumed. For all three species, OH concentrations are found to be a factor of 2 to 3 higher than calculated by models for atmospheric conditions with low NO concentrations. Current state-of-the-art models increased already OH production for isoprene and methacrolein oxidation by including additional reaction pathways. The study here shows that this is also needed for the MVK oxidation scheme.

Data availability. Data of the experiments in the SAPHIR chamber used in this work is available on the EUROCHAMP data homepage (https://data.eurochamp.org/, last access: April 2018).

The Supplement related to this article is available online at https://doi.org/10.5194/acp-18-8001-2018-supplement.

Competing interests. The authors declare to have no competing interests.

Acknowledgements. This project has received funding from the European Research Council (ERC) under the European Union's Horizon 2020 research and innovation programme (SARLEP grant agreement No. 681529) and from the European Commission (EC) under the European Union's Horizon 2020 research and innovation programme (Eurochamp 2020 grant agreement No. 730997). The authors thank the Forschungszentrum Jülich for travel support under the project "Seed Money". Frank N. Keutsch and Alex Zaytsev were supported by the National Science Foundation (AGS 1628491 and 1628530). Martin Breitenlechner was supported by the Austrian Science Fund (FWF), Erwin Schrödinger Stipendium, Grant No. J-3900. The authors thank Thomas Mentel, Yare Baker and Sungah Kang from Forschungszentrum Jülich for supporting the HO_2 CIMS measurements.

The article processing charges for this open-access
publication were covered by a Research
Centre of the Helmholtz Association.

Edited by: Sergey A. Nizkorodov
Reviewed by: two anonymous referees

References

Aschmann, S. M., Arey, J., and Atkinson, R.: OH radical formation from the gas-phase reactions of O_3 with methacrolein and methyl vinyl ketone, Atmos. Environ., 30, 2939–2943, https://doi.org/10.1016/1352-2310(96)00013-1, 1996.

Atkinson, R., Baulch, D. L., Cox, R. A., Crowley, J. N., Hampson, R. F., Hynes, R. G., Jenkin, M. E., Rossi, M. J., Troe, J., and Subcommittee, I.: Evaluated kinetic and photochemical data for atmospheric chemistry: Volume II – gas phase reactions of organic species, Atmos. Chem. Phys., 6, 3625–4055, https://doi.org/10.5194/acp-6-3625-2006, 2006.

Bohn, B. and Zilken, H.: Model-aided radiometric determination of photolysis frequencies in a sunlit atmosphere simulation chamber, Atmos. Chem. Phys., 5, 191–206, https://doi.org/10.5194/acp-5-191-2005, 2005.

Bohn, B., Rohrer, F., Brauers, T., and Wahner, A.: Actinometric measurements of NO_2 photolysis frequencies in the atmosphere simulation chamber SAPHIR, Atmos. Chem. Phys., 5, 493–503, https://doi.org/10.5194/acp-5-493-2005, 2005.

Cox, R. A., Munk, J., Nielsen, O. J., Pagsberg, P., and Ratajczak, E.: Ultraviolet absorption spectra and kinetics of acetonyl and acetonylperoxy radicals, Chem. Phys. Lett., 173, 206–210, https://doi.org/10.1016/0009-2614(90)80079-S, 1990.

Crounse, J. D., Paulot, F., Kjaergaard, H. G., and Wennberg, P. O.: Peroxy radical isomerization in the oxidation of isoprene, Phys. Chem. Chem. Phys., 13, 13607–13613, https://doi.org/10.1039/C1CP21330J, 2011.

Crounse, J. D., Knap, H. C., Ornso, K. B., Jorgensen, S., Paulot, F., Kjaergaard, H. G., and Wennberg, P. O.: On the atmospheric fate of methacrolein: 1. Peroxy radical isomerization following addition of OH and O_2, J. Phys. Chem. A, 116, 5756–5762, https://doi.org/10.1021/jp211560u, 2012.

D'Ambro, E. L., Moller, K. H., Lopez-Hilfiker, F. D., Schobesberger, S., Liu, J., Shilling, J. E., Lee, B. H., Kjaergaard, H. G., and Thornton, J. A.: Isomerization of second-generation isoprene peroxy radicals: epoxide formation and implications for secondary organic aerosol yields, Environ Sci. Technol., 51, 4978–4987, https://doi.org/10.1021/acs.est.7b00460, 2017.

Dillon, T. J. and Crowley, J. N.: Direct detection of OH formation in the reactions of HO_2 with $CH_3C(O)O_2$ and other substituted peroxy radicals, Atmos. Chem. Phys., 8, 4877–4889, https://doi.org/10.5194/acp-8-4877-2008, 2008.

Dorn, H.-P., Brandenburger, U., Brauers, T., and Hausmann, M.: A new in-situ laser long-path absorption instrument for the measurement of tropospheric OH radicals, J. Atmos. Sci., 52, 3373–3380, 1995.

Dunning, T. H.: Gaussian basis sets for use in correlated molecular calculations. I. The atoms boron through neon and hydrogen, J. Chem. Phys., 90, 1007–1023, https://doi.org/10.1063/1.456153, 1989.

Eurochamp: Database of Atmospheric Simulation Chamber Studies, available at: https://data.eurochamp.org/data-access/chamber-experiments/, last accesss: April 2018.

Frisch, M. J., Trucks, G. W., Schlegel, H. B., Scuseria, G. E., Robb, M. A., Cheeseman, J. R., Scalmani, G., Barone, V., Mennucci, B., Petersson, G. A., Nakatsuji, H., Caricato, M., Li, X., Hratchian, H. P., Izmaylov, A. F., Bloino, J., Zheng, G., Sonnenberg, J. L., Hada, M., Ehara, M., Toyota, K., Fukuda, R., Hasegawa, J., Ishida, M., Nakajima, T., Honda, Y., Kitao, O., Nakai, H., Vreven, T., A., M. J. J., Peralta, J. E., Ogliaro, F., Bearpark, M., Heyd, J. J., Brothers, E., Kudin, K. N., Staroverov, V. N., Keith, T., Kobayashi, R., Normand, J., Normand, J., Raghavachari, K., Rendell, A., Burant, J. C., Iyengar, S. S., Tomasi, J., Cossi, M., Rega, N., Millam, J. M., Klene, M., Knox, J. E., Cross, J. B., Bakken, V., Adamo, C., Jaramillo, J., Gomperts, R., Stratmann, R. E., Yazyev, O., Austin, A. J., Cammi, R., Pomelli, C., Ochterski, J. W., Martin, R. L., Morokuma, K., Zakrzewski, V. G., Voth, G. A., Salvador, P., Dannenberg, J. J., Dapprich, S., Daniels, A. D., Farkas, O., Foresman, J. B., Ortiz, J. V., Cioslowski, J., Fox, D. J., and Pople, J. A.: Gaussian 09, Revision B.01, Gaussian Inc., Wallington CT., 2010.

Fuchs, H., Hofzumahaus, A., and Holland, F.: Measurement of tropospheric RO_2 and HO_2 radicals by a laser-induced fluorescence instrument, Rev. Sci. Instrum., 79, 084104, https://doi.org/10.1063/1.2968712, 2008.

Fuchs, H., Dube, W. P., Lerner, B. M., Wagner, N. L., Williams, E. J., and Brown, S. S.: A sensitive and versatile detector for atmospheric NO_2 and NO_x based on blue diode laser cavity ring-down spectroscopy, Environ. Sci. Technol., 43, 7831–7836, https://doi.org/10.1021/es902067h, 2009.

Fuchs, H., Bohn, B., Hofzumahaus, A., Holland, F., Lu, K. D., Nehr, S., Rohrer, F., and Wahner, A.: Detection of HO_2 by laser-induced fluorescence: calibration and interferences from RO_2 radicals, Atmos. Meas. Tech., 4, 1209–1255, https://doi.org/10.5194/amt-4-1209-2011, 2011.

Fuchs, H., Dorn, H. P., Bachner, M., Bohn, B., Brauers, T., Gomm, S., Hofzumahaus, A., Holland, F., Nehr, S., Rohrer, F., Tillmann, R., and Wahner, A.: Comparison of OH concentration measurements by DOAS and LIF during SAPHIR chamber experiments at high OH reactivity and low NO concentration, Atmos. Meas. Tech., 5, 1611–1626, https://doi.org/10.5194/amt-5-1611-2012, 2012.

Fuchs, H., Hofzumahaus, A., Rohrer, F., Bohn, B., Brauers, T., Dorn, H.-P., Häseler, R., Holland, F., Kaminski, M., Li, X., Lu, K., Nehr, S., Tillmann, R., Wegener, R., and Wahner, A.: Experimental evidence for efficient hydroxyl radical regeneration in isoprene oxidation, Nat. Geosci., 6, 1023–1026, https://doi.org/10.1038/NGEO1964, 2013.

Fuchs, H., Acir, I. H., Bohn, B., Brauers, T., Dorn, H. P., Häseler, R., Hofzumahaus, A., Holland, F., Kaminski, M., Li, X., Lu, K., Lutz, A., Nehr, S., Rohrer, F., Tillmann, R., Wegener, R., and Wahner, A.: OH regeneration from methacrolein oxidation investigated in the atmosphere simulation chamber SAPHIR, Atmos. Chem. Phys., 14, 7895–7908, https://doi.org/10.5194/acp-14-7895-2014, 2014.

Fuchs, H., Tan, Z., Hofzumahaus, A., Broch, S., Dorn, H. P., Holland, F., Künstler, C., Gomm, S., Rohrer, F., Schrade, S., Tillmann, R., and Wahner, A.: Investigation of potential interferences in the detection of atmospheric RO_X radicals by laser-induced fluorescence under dark conditions, Atmos. Meas. Tech., 9, 1431–1447, https://doi.org/10.5194/amt-9-1431-2016, 2016.

Fuchs, H., Novelli, A., Rolletter, M., Hofzumahaus, A., Pfannerstill, E. Y., Kessel, S., Edtbauer, A., Williams, J., Michoud, V., Dusanter, S., Locoge, N., Zannoni, N., Gros, V., Truong, F., Sarda-Esteve, R., Cryer, D. R., Brumby, C. A., Whalley, L. K., Stone, D., Seakins, P. W., Heard, D. E., Schoemaecker, C., Blocquet, M., Coudert, S., Batut, S., Fittschen, C., Thames, A. B., Brune, W. H., Ernest, C., Harder, H., Muller, J. B. A., Elste, T., Kubistin, D., Andres, S., Bohn, B., Hohaus, T., Holland, F., Li, X., Rohrer, F., Kiendler-Scharr, A., Tillmann, R., Wegener, R., Yu, Z., Zou, Q., and Wahner, A.: Comparison of OH reactivity measurements in the atmospheric simulation chamber SAPHIR, Atmos. Meas. Tech., 10, 4023–4053, https://doi.org/10.5194/amt-10-4023-2017, 2017.

Galloway, M. M., Huisman, A. J., Yee, L. D., Chan, A. W. H., Loza, C. L., Seinfeld, J. H., and Keutsch, F. N.: Yields of oxidized volatile organic compounds during the OH radical initiated oxidation of isoprene, methyl vinyl ketone, and methacrolein under high-NO_X conditions, Atmos. Chem. Phys., 11, 10779–10790, https://doi.org/10.5194/acp-11-10779-2011, 2011.

Grosjean, D., Williams, E. L., and Grosjean, E.: Atmospheric chemistry of isoprene and of its carbonyl products, Environ Sci. Technol., 27, 830–840, https://doi.org/10.1021/es00042a004, 1993.

Guenther, A. B., Jiang, X., Heald, C. L., Sakulyanontvittaya, T., Duhl, T., Emmons, L. K., and Wang, X.: The model of emissions of gases and aerosols from nature version 2.1 (MEGAN2.1): an extended and updated framework for modeling biogenic emissions, Geosci. Model Dev., 5, 1471–1492, https://doi.org/10.5194/gmd-5-1471-2012, 2012.

Hansen, R. F., Lewis, T. R., Graham, L., Whalley, L. K., Seakins, P. W., Heard, D. E., and Blitz, M. A.: OH production from the photolysis of isoprene-derived peroxy radicals: cross-sections, quantum yields and atmospheric implications, Phys. Chem. Chem. Phys., 19, 2332–2345, https://doi.org/10.1039/C6CP06718B, 2017.

Hens, K., Novelli, A., Martinez, M., Auld, J., Axinte, R., Bohn, B., Fischer, H., Keronen, P., Kubistin, D., Nölscher, A. C., Oswald, R., Paasonen, P., Petäjä, T., Regelin, E., Sander, R., Sinha, V., Sipilä, M., Taraborrelli, D., Tatum Ernest, C., Williams, J., Lelieveld, J., and Harder, H.: Observation and modelling of HO_X radicals in a boreal forest, Atmos. Chem. Phys., 14, 8723–8747, https://doi.org/10.5194/acp-14-8723-2014, 2014.

Hofzumahaus, A., Rohrer, F., Lu, K., Bohn, B., Brauers, T., Chang, C.-C., Fuchs, H., Holland, F., Kita, K., Kondo, Y., Li, X., Lou, S., Shao, M., Zeng, L., Wahner, A., and Zhang, Y.: Amplified trace gas removal in the troposphere, Science, 324, 1702–1704, https://doi.org/10.1126/science.1164566, 2009.

Kaminski, M., Fuchs, H., Acir, I. H., Bohn, B., Brauers, T., Dorn, H. P., Häseler, R., Hofzumahaus, A., Li, X., Lutz, A., Nehr, S., Rohrer, F., Tillmann, R., Vereecken, L., Wegener, R., and Wahner, A.: Investigation of the β-pinene photooxidation by OH in the atmosphere simulation chamber SAPHIR, Atmos. Chem. Phys., 17, 6631–6650, https://doi.org/10.5194/acp-17-6631-2017, 2017.

Karl, M., Dorn, H.-P., Holland, F., Koppmann, R., Poppe, D., Rupp, L., Schaub, A., and Wahner, A.: Product study of the reaction of OH radicals with isoprene in the atmosphere simulation chamber SAPHIR, J. Atmos. Chem., 55, 167–187, https://doi.org/10.1007/s10874-006-9034-x, 2006.

Karunanandan, R., Hölscher, D., Dillon, T. J., Horowitz, A., Crowley, J. N., Vereecken, L., and Peeters, J.: Reaction of HO with glycolaldehyde $HOCH_2CHO$: Rate coefficients (240–362 K) and mechanism, J. Chem. Phys. A, 111, 897–908, https://doi.org/10.1021/jp0649504, 2007.

Kim, S., Wolfe, G. M., Mauldin, L., Cantrell, C., Guenther, A., Karl, T., Turnipseed, A., Greenberg, J., Hall, S. R., Ullmann, K., Apel, E., Hornbrook, R., Kajii, Y., Nakashima, Y., Keutsch, F. N., DiGangi, J. P., Henry, S. B., Kaser, L., Schnitzhofer, R., Graus, M., and Hansel, A.: Evaluation of HO_X sources and cycling using measurement-constrained model calculations in a 2-methyl-3-butene-2-ol (MBO) and monoterpene (MT) dominated ecosystem, Atmos. Chem. Phys., 13, 2031–2044, https://doi.org/10.5194/acp-13-2031-2013, 2013.

Lelieveld, J., Butler, T. M., Crowley, J. N., Dillon, T. J., Fischer, H., Ganzeveld, L., Harder, H., Lawrence, M. G., Martinez, M., Taraborrelli, D., and Williams, J.: Atmospheric oxidation capacity sustained by a tropical forest, Nature, 452, 737–740, https://doi.org/10.1038/nature06870, 2008.

Lew, M. M., Dusanter, S., and Stevens, P. S.: Measurement of interferences associated with the detection of the hydroperoxy radical in the atmosphere using laser-induced fluorescence, Atmos. Meas. Tech., 11, 95–108, https://doi.org/10.5194/amt-11-95-2018, 2018.

Lou, S., Holland, F., Rohrer, F., Lu, K., Bohn, B., Brauers, T., Chang, C. C., Fuchs, H., Häseler, R., Kita, K., Kondo, Y., Li, X., Shao, M., Zeng, L., Wahner, A., Zhang, Y., Wang, W., and Hofzumahaus, A.: Atmospheric OH reactivities in the Pearl River Delta – China in summer 2006: measurement and model results, Atmos. Chem. Phys., 10, 11243–11260, https://doi.org/10.5194/acp-10-11243-2010, 2010.

Lu, K. D., Rohrer, F., Holland, F., Fuchs, H., Bohn, B., Brauers, T., Chang, C. C., Häseler, R., Hu, M., Kita, K., Kondo, Y., Li, X., Lou, S. R., Nehr, S., Shao, M., Zeng, L. M., Wahner, A., Zhang, Y. H., and Hofzumahaus, A.: Observation and modelling of OH and HO_2 concentrations in the Pearl River Delta 2006: a missing OH source in a VOC rich atmosphere, Atmos. Chem. Phys., 12, 1541–1569, https://doi.org/10.5194/acp-12-1541-2012, 2012.

Mao, J., Ren, X., Brune, W. H., Van Duin, D. M., Cohen, R. C., Park, J. H., Goldstein, A. H., Paulot, F., Beaver, M. R., Crounse, J. D., Wennberg, P. O., DiGangi, J. P., Henry, S. B., Keutsch, F. N., Park, C., Schade, G. W., Wolfe, G. M., and Thornton, J. A.: Insights into hydroxyl measurements and atmospheric oxidation in a California forest, Atmos. Chem. Phys., 12, 8009–8020, https://doi.org/10.5194/acp-12-8009-2012, 2012.

Martin, J. M. L.: Ab initio total atomization energies of small molecules – towards the basis set limit, Chem. Phys. Lett., 259, 669–678, https://doi.org/10.1016/0009-2614(96)00898-6, 1996.

MCM: Master Chemical Mechanism, available at: http://mcm.leeds.ac.uk/MCM/, last access: May 2017.

Nölscher, A. C., Williams, J., Sinha, V., Custer, T., Song, W., Johnson, A. M., Axinte, R., Bozem, H., Fischer, H., Pouvesle, N., Phillips, G., Crowley, J. N., Rantala, P., Rinne, J., Kulmala, M., Gonzales, D., Valverde-Canossa, J., Vogel, A., Hoffmann, T., Ouwersloot, H. G., Vila-Guerau de Arellano, J., and Lelieveld, J.: Summertime total OH reactivity measurements from boreal forest during HUMPPA-COPEC 2010, Atmos. Chem. Phys., 12, 8257–8270, https://doi.org/10.5194/acp-12-8257-2012, 2012.

Novelli, A., Hens, K., Tatum Ernest, C., Kubistin, D., Regelin, E., Elste, T., Plass-Dülmer, C., Martinez, M., Lelieveld, J., and Harder, H.: Characterisation of an inlet pre-injector laser-induced fluorescence instrument for the measurement of atmospheric hydroxyl radicals, Atmos. Meas. Tech., 7, 3413–3430, https://doi.org/10.5194/amt-7-3413-2014, 2014.

Paulson, S. E., Chung, M., Sen, A. D., and Orzechowska, G.: Measurement of OH radical formation from the reaction of ozone with several biogenic alkenes, J. Geophys. Res., 103, 25533–25539, https://doi.org/10.1029/98JD01951, 1998.

Peeters, J., Nguyen, T. L., and Vereecken, L.: HO_X radical regeneration in the oxidation of isoprene, Phys. Chem. Chem. Phys., 11, 5935–5939, https://doi.org/10.1039/b908511d, 2009.

Peeters, J., Müller, J.-F., Stavrakou, T., and Nguyen, V. S.: Hydroxyl radical recycling in isoprene oxidation driven by hydrogen bonding and hydrogen tunneling: The upgraded LIM1 mechanism, J. Phys. Chem. A, 118, 8625–8643, https://doi.org/10.1021/jp5033146, 2014.

Praske, E., Crounse, J. D., Bates, K. H., Kurten, T., Kjaergaard, H. G., and Wennberg, P. O.: Atmospheric fate of methyl vinyl ketone: Peroxy radical reactions with NO and HO_2, J. Phys. Chem. A, 119, 4562–4572, https://doi.org/10.1021/jp5107058, 2015.

Purvis, G. D. and Bartlett, R. J.: A full coupled-cluster singles and doubles model: The inclusion of disconnected triples, J. Chem. Phys., 76, 1910–1918, https://doi.org/10.1063/1.443164, 1982.

Rickly, P. and Stevens, P. S.: Measurements of a potential interference with laser-induced fluorescence measurements of ambient OH from the ozonolysis of biogenic alkenes, Atmos. Meas. Tech., 11, 1–16, https://doi.org/10.5194/amt-11-1-2018, 2018.

Rohrer, F., Bohn, B., Brauers, T., Brüning, D., Johnen, F.-J., Wahner, A., and Kleffmann, J.: Characterisation of the photolytic HONO-source in the atmosphere simulation chamber SAPHIR, Atmos. Chem. Phys., 5, 2189–2201, https://doi.org/10.5194/acp-5-2189-2005, 2005.

Sanchez, J., Tanner, D. J., Chen, D., Huey, L. G., and Ng, N. L.: A new technique for the direct detection of HO_2 radicals using bromide chemical ionization mass spectrometry (Br-CIMS): initial characterization, Atmos. Meas. Tech., 9, 3851–3861, https://doi.org/10.5194/amt-9-3851-2016, 2016.

Schlosser, E., Brauers, T., Dorn, H.-P., Fuchs, H., Häseler, R., Hofzumahaus, A., Holland, F., Wahner, A., Kanaya, Y., Kajii, Y., Miyamoto, K., Nishida, S., Watanabe, K., Yoshino, A., Kubistin, D., Martinez, M., Rudolf, M., Harder, H., Berresheim, H., Elste, T., Plass-Dülmer, C., Stange, G., and Schurath, U.: Technical Note: Formal blind intercomparison of OH measurements: results from the international campaign HOxComp, Atmos. Chem. Phys., 9, 7923–7948, https://doi.org/10.5194/acp-9-7923-2009, 2009.

St. Clair, J. M., Rivera, J. C., Crounse, J. D., Knap, H. C., Bates, K. H., Teng, A. P., Jørgensen, S., Kjaergaard, H. G., Keutsch, F. N., and Wennberg, P. O.: Kinetics and products of the reaction of the first-generation isoprene hydroxy hydroperoxide (ISOPOOH) with OH, J. Phys. Chem. A, 120, 1441–1451, https://doi.org/10.1021/acs.jpca.5b06532, 2015.

Tan, D., Faloona, I., Simpas, J. B., Brune, W., Shepson, P. B., Couch, T. L., Summer, A. L., Carroll, M. A., Thornberry, T., Apel, E., Riemer, D., and Stockwell, W.: HO_X budget in a deciduous forest: results from the PROPHET summer 1998 campaign, J. Geophys. Res., 106, 24407–24427, https://doi.org/10.1029/2001JD900016, 2001.

Tuazon, E. C. and Atkinson, R.: A product study of the gas-phase reaction of methyl vinyl ketone with the OH radical in the presence of NO_X, Int. J. Chem. Kin., 21, 1141–1152, https://doi.org/10.1002/kin.550211207, 1989.

Vereecken, L. and Peeters, J.: The 1,5-H-shift in 1-butoxy: A case study in the rigorous implementation of transition state theory for a multirotamer system, J. Chem. Phys., 119, 5159–5170, https://doi.org/10.1063/1.1597479, 2003.

Vereecken, L. and Peeters, J.: Decomposition of substituted alkoxy radicals-part I: a generalized structure-activity relationship for reaction barrier heights, Phys. Chem. Chem. Phys., 11, 9062–9074, https://doi.org/10.1039/B909712K, 2009.

Veres, P. R., Roberts, J. M., Wild, R. J., Edwards, P. M., Brown, S. S., Bates, T. S., Quinn, P. K., Johnson, J. E., Zamora, R. J., and de Gouw, J.: Peroxynitric acid (HO_2NO_2) measurements during the UBWOS 2013 and 2014 studies using iodide ion chemical ionization mass spectrometry, Atmos. Chem. Phys., 15, 8101–8114, https://doi.org/10.5194/acp-15-8101-2015, 2015.

Wennberg, P. O., Bates, K. H., Crounse, J. D., Dodson, L. G., McVay, R. C., Mertens, L. A., Nguyen, T. B., Praske, E., Schwantes, R. H., Smarte, M. D., St Clair, J. M., Teng, A. P., Zhang, X., and Seinfeld, J. H.: Gas-Phase reactions of isoprene and its major oxidation products, Chem. Rev., 18, 3337–3390, https://doi.org/10.1021/acs.chemrev.7b00439, 2018.

Whalley, L. K., Edwards, P. M., Furneaux, K. L., Goddard, A., Ingham, T., Evans, M. J., Stone, D., Hopkins, J. R., Jones, C. E., Karunaharan, A., Lee, J. D., Lewis, A. C., Monks, P. S., Moller, S. J., and Heard, D. E.: Quantifying the magnitude of a missing hydroxyl radical source in a tropical rainforest, Atmos. Chem. Phys., 11, 7223–7233, https://doi.org/10.5194/acp-11-7223-2011, 2011.

Whalley, L. K., Blitz, M. A., Desservettaz, M., Seakins, P. W., and Heard, D. E.: Reporting the sensitivity of laser-induced fluorescence instruments used for HO_2 detection to an interference from RO_2 radicals and introducing a novel approach that enables HO_2 and certain RO_2 types to be selectively measured, Atmos. Meas. Tech., 6, 3425–3440, https://doi.org/10.5194/amt-6-3425-2013, 2013.

Winiberg, F. A. F., Dillon, T. J., Orr, S. C., Gro ß, C. B. M., Bejan, I., Brumby, C. A., Evans, M. J., Smith, S. C., Heard, D. E., and Seakins, P. W.: Direct measurements of OH and other product yields from the HO_2 + $CH_3C(O)O_2$ reaction, Atmos. Chem. Phys., 16, 4023–4042, https://doi.org/10.5194/acp-16-4023-2016, 2016.

Wolfe, G. M., Crounse, J. D., Parrish, J. D., St. Clair, J. M., Beaver, M. R., Paulot, F., Yoon, T., Wennberg, P. O., and Keutsch, F. N.: Photolysis, OH reactivity and ozone reactivity of a proxy for isoprene-derived hydroperoxyenals, Phys. Chem. Chem. Phys., 14, 7276–7286, https://doi.org/10.1039/C2CP40388A, 2012.

Zhao, Y. and Truhlar, D. G.: The M06 suite of density functionals for main group thermochemistry, thermochemical kinetics, noncovalent interactions, excited states, and transition elements: two new functionals and systematic testing of four M06-class functionals and 12 other functionals, Theor. Chem. Account., 120, 215–241, https://doi.org/10.1007/s00214-007-0310-x, 2008.

Zheng, J. and Truhlar, D. G.: Quantum thermochemistry: Multistructural method with torsional anharmonicity based on a coupled torsional potential, J. Chem. Theory Comput., 9, 1356–1367, https://doi.org/10.1021/ct3010722, 2013.